Journal of the Korea Concrete Institute
Vol.17 No.5, pp.857~868, October, 2005

A Numerical Model for the Freeze-Thaw Damages in Concrete Structures

Tae-Jun Cho[1)*]

[1)]*Dept. of Civil & Env. Eng., Cheongju University, Cheongju, Chungbuk 360-170, Korea*

(Received April 18, 2005, Accepted July 10, 2005)

Abstract

This paper deals with the accumulated damage in concrete structures due to the cyclic freeze-thaw as an environmental load. The cyclic ice body nucleation and growth processes in porous systems are affected by the thermo-physical and mass transport properties, and gradients of temperature and chemical potentials. Furthermore, the diffusivity of deicing chemicals shows significantly higher value under cyclic freeze-thaw conditions. Consequently, the disintegration of concrete structures is aggravated at marine environments, higher altitudes, and northern areas. However, the properties of cyclic freeze-thaw with crack growth and diffusion of chloride ion effects are hard to be identified in tests, and there has been no analytic model for the combined degradations. The main objective is to determine the driving force and evaluate the reduced strength and stiffness by freeze-thaw. For the development of computational model of those coupled deterioration, micro-pore structure characterization, pore pressure based on the thermodynamic equilibrium, time and temperature dependent super-cooling with or without deicing salts, nonlinear-fracture constitutive relation for the evaluation of internal damage, and the effect of entrained air pores (EA) has been modeled numerically. As a result, the amount of ice volume with temperature dependent surface tensions, freezing pressure and resulting deformations, and cycle and temperature dependent pore volume has been calculated and compared with available test results. The developed computational program can be combined with DuCOM, which can calculate the early aged strength, heat of hydration, micro-pore volume, shrinkage, transportation of free water in concrete. Therefore, the developed model can be applied to evaluate those various practical degradation cases as well.

Keywords: freeze-thaw, micro cracking, pore structure, mortar, numerical analysis

1. Introduction

One of the most widely shredded misconceptions about freeze-thaw induced damage in concrete might be a surface scaling. Various experimental results show that the scaling after hundreds of cyclic freeze-thaw test is less than 5% in mass ratio[1)]. A much bigger damage might come from the accumulated micro-cracking in the concrete, which is the result of freezing and thawing pressures. Therefore, the analytical evaluation of the accumulated damage needs to be started from the modeling of pore structures of concrete.

One important phenomenon for the estimation of freeze-thaw can be the transportation of water under the cyclic temperature loads. Through the in and outflow of water and vapor to and from concrete, the total volume and strain are varied. Depending on the temperature variation, they can be evaluated.

The types of damage can be divided as surface scaling, internal damage, and internal attack of aggregate. Surface scaling is the loss of paste and mortar from the surface of concrete. In extreme cases, the loss of mortar will be progressive, resulting in the loosening of coarse aggregate and the gradual reduction of the concrete section. Surface scaling is generally found associated with the use of de-icing salts, through mild scaling can occur even when no deicing are used.

Internal attack of the paste of the concrete results in the crumbling and eventually the total deterioration of the con-

* *Corresponding author*
Email address: taejun@cju.ac.kr

crete. Development of pressures and cracking, accompanied by a local redistribution of moisture during freezing, followed by either absorption of moisture from outside the concrete or internal redistribution of moisture during thawing, the accumulated cracking leads to the crumbling of the concrete. It is hard to be found in situ, because it needs long term exposure conditions.

Concrete made with aggregates having a preponderance of pores in the 0.0 to 0.2 μm diameter range may be susceptible to freeze-thaw attack of the aggregates in the concrete. It is generally found associated with considerable moistures around the specimen are required. These phenomena (internal attack of aggregate, D-cracking) require ten to fifteen years of exposure condition.

To identify the accumulated damage in concrete structures by cyclic freeze-thaw, the following numerical models have been studied:

- Determining the driving force of freeze-thaw and evaluating the reduced strength and stiffness
- Development of computational models for micro-pore structure characterization, pore pressure based on the thermodynamic equilibrium, time and temperature dependent super-cooling with or without deicing salts, nonlinear-fracture constitutive relationship for the evaluation of internal damage, and the resisting effect of entrained air pores

2. Chemical potential of ice and water in Porous systems

The chemical potential of a substance j in a system may be defined as the change of the Gibbs energy of the entire system which an infinitesimal change in the amount n_j of substance j causes:

$$\mu_j = \left(\frac{\partial G}{\partial n_j} \right) \tag{1}$$

The Gibbs energy of an entire system may then be expressed as:

$$G = \sum_j n_j \mu_j \tag{2}$$

For one-component, multi-phase system at internal equilibrium, a distribution of the component in the different phases is adopted so that the system's Gibbs energy comes to a minimum.

Chemical potential of pure substances in bulk i^{th} infinitesimal change in pressure and temperature, the Gibbs energy of a closed system (doing no non-expansion work) changes as follows:

$$dG = Vdp - SdT \tag{3}$$

For a pure substance, put on a molar scale, this leads to a change in chemical potential:

$$d\mu = \mu - \mu_o = V_m dP - S_m dT \tag{4}$$

For two separate systems to be in equilibrium, it is necessary that their Gibbs energies be equal. For two systems, each of which is a pure substance, this means that the chemical potentials of the two substances must be equal.

The effect of surface energy on the chemical potential of water is dependent on the free energies of the interfaces and surfaces that it comprises so that

$$G = G_o + \sum \sigma_i A_i \tag{5}$$

in which G_0 is the free energy of the bulk phases and A_i is the area of the interfaces/surfaces of free energies. Thus, when interface area within a system changes, the free energy of the system changes. For example, water entering a narrow pore in a matrix of solid material causes a change in interface energies. Before entering, there is a matrix–air interface. Afterwards, there is a matrix–water interface. This change in free energy of the system is caused by the addition of water and thus, the chemical potential of the water in the system is:

$$d\mu = \mu_o + \Delta\sigma dA_m \tag{6}$$

with μ_0 the chemical potential in the bulk state, the interface energy change and dA_m the change of interface area per mole of added water. The interface energy change is defined:

$$\Delta\sigma = \sigma_f - \sigma_i \tag{7}$$

in which f is the interface energy of the final interface and that of the initial one. In capillary suction, the matrix–water interface energy is lower than that of the matrix–air interface. Uptake of water thus causes a decrease in the free energy of the system (bulk water + solid) and so the process is spontaneous.

In the case of a cylindrical pore of circular cross section, the term dA (omitting the area of the pore ends) is:

$$dA = 2\pi r dx \tag{8}$$

in which r is the pore radius and dx is the depth of water penetration. dx is calculated from the volume of water that enters the pore:

$$dV = V_{m,l} dn_l = \pi r^2 dx \tag{9}$$

with $V_{m,l}$ the molar volume of water and d_{nl} the change of water content. The change of interface area per mole of water that enters the pore, $dA_{,ms}$, thus becomes:

The equilibrium between a small ice body and bulk water, the chemical potential of a small ice body, is obtained from Eq.10 and that of bulk water is obtained from Eq.4. From these equations, it can be seen that the chemical potential of an ice body will exceed that of bulk water if its surface area is sufficiently large. Such an ice body will be unstable and will melt. Comparing the chemical potentials, we may find the temperature dependence of the size of a stable ice body in its own melt from:

$$-S_{m,s} dT_s + V_{m,s} dP_s + \sigma_{s-l} dA_{m,s} = -S_{m,s} dT + V_{m,l} dP_l \tag{10}$$

Assuming the ice body to be spherical, the interface area changes with the number of moles of ice according to:

$$dA_{m,s} = \frac{2V_{m,s}}{r_s} d\eta_s \tag{11}$$

in which r_s is the radius of the ice sphere. The interface energy σ_{s-l} is that of an ice–water interface, which is approximately 0.033 J/m^2. Above, "-" sign was used to allow for changes in type of interface following the different processes. Here, the interface energy remains constant (only the interface area changes) and thus the "-" sign is omitted. Assuming the pressures remain atmospheric and the temperatures of the two phases to be equal, we find:

$$\sigma_{s-l} \frac{2V_{m,s}}{r_s} = (S_{m,s} - S_{m,l}) dT \tag{12}$$

The right hand side of equation has to be integrated (from the temperature of fusion in bulk to the actual temperature), taking the temperature dependence of the molar entropies into consideration. The entropy of a substance varies with temperature in accordance with:

$$S(T_f) = S(T_i) + \int_{Ti}^{Tf} \frac{C_p(T)}{T} dT \tag{13}$$

The heat capacity may, within reasonable intervals, be expressed with an expression in the form:

$$C_p = AT + B \tag{14}$$

(The amount of energy required to raise the temperature of 1 g of material 1°C water is 4200J/(kg °C), the heat capacity of ice is 2100 J / (kg °C), the heat of fusion of water is 3.4 x 10^5 J/kg, and its heat of vaporization is 2.3 x 10^6 J/kg.)

The cooling of liquid below its freezing temperature without the formation of the solid phase is calculated considering the potential equilibrium of solid and liquid:

$$-S_{m,s} dT + V_{m,s} dP + \sigma_{s-l} dA_{m,s} = -S_{m,l} dT + V_{m,l} dP \tag{15}$$

$$\sigma_{s-l} \frac{2V_{m,s}}{r_s} = (S_{m,s} - S_{m,l}) dT, S(T_f) = S(T_i) + \int_{Ti}^{Tf} \frac{C_p(T)}{T} dT \tag{16}$$

Where, $C_p(T)^{ice} = -0.05987T + 92.3687$

$$\Delta(\Delta\mu) = \int_{Tref}^{T} (S_{m,s}(T) - S_{m,l}(T)) dT = 0.0997T^2 - 76.4532T + 13444.483 \tag{17}$$

Or, approximately,

$$S_{m,s} dT - S_{m,l} dT = -\frac{\Delta H_{fus}}{T}. \tag{18}$$

Finally, the minimum freezable radius of a pore is:

$$r_s = \frac{2\sigma_{s-l} V_{m,s}}{\int_{To}^{T} (S_{m,s} - S_{m,l}) dT} \tag{19}$$

Which mean unfreezable, super cooled, water in lower temperature than 0°C.

3. Freezing in micro porestructure

3.1 Micro porestructure

Hydration and microstructural informaion are obtained-from the analysis results of DuCOM[2], which calculates the early aged strength, heat of hydration, micro-pore volume, shrinkage, corrosion of embedded steel and transportation

of free water in concrete[3].

In DuCOM, for the hydration model, multi-component chemical reactions and compounds have been considered as input data. Based on solidification theory, the reactants, mainly cement, aggregate and water, produce C-S-H gel structures, as modeled schematically in a cluster at Fig. 1.

Fig.1 shows the solidification process of cement paste is idealized by the formation of finite age-independent structural elements called clusters. The aging process of cement paste is represented by the solidification of new cluster. As hydration proceeds, number of clusters increases (Fig. 2).

The surface areas of capillary and gel pores can be computed using a bi-model R-R porosity distribution f(r) which gives the total porosity function is assumed. Thus, we have,

$$\phi(r) = \phi_l + \phi_g V_g(r) + \phi_c V_c(r) \tag{20}$$

where r: pore radius. $V_g(r)$ and $V_c(r)$ represent the fractional pore volumes of gel and capillary pores in the distribution, respectively (Fig. 3).

$$V_i(r) = 1 - \exp(-B_i r) \quad (0 \le V_g(r) \le 1) \tag{21}$$

$$dV_i = B_i r \exp(-B_i r) d\ln r \tag{22}$$

In the Fig. 3, the distribution parameters B_i represent the peak of the porosity distribution on a logarithmic scale. If we assume a cylindrical pore shape in such a distribution, these parameters can be easily obtained from the computed porosity and surface area values for the capillary and micro-gel regions.

3.2 Surface energy and freezable water

The minimum freezable pore size had been obtained by assuming cylindrical pore structure in isobaric condition approximately[4].

$$r_T = -\frac{2T_O \gamma_{lv} V_l}{\Delta H_{fus} \Delta T} \tag{23}$$

Or integrating entropy for the considered temperature range:

$$r_s = \frac{2\gamma_{S-L} V_{m,s}}{0.0997T^2 - 76.4532T + 13444.483} \tag{4}$$

where, $V_{m,s}$ =19.65*10^{-6} m^3/mol : molar volume of ice

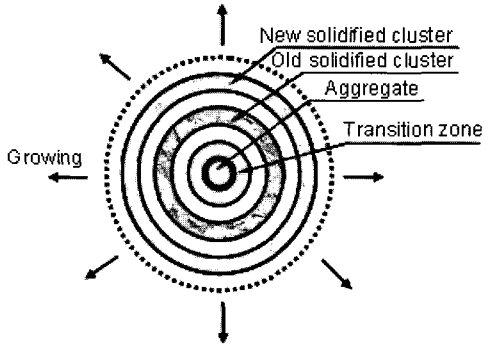

Fig. 1 Schematic representation of Hydration solidification process

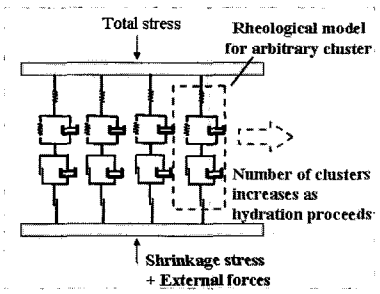

Fig. 2 Number of clusters increases as proceeds

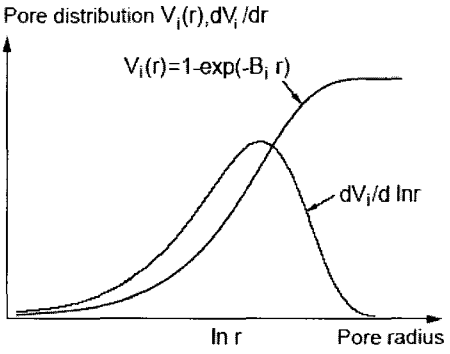

Fig. 3 Cumulative distribution function and density function for the porosity diagram

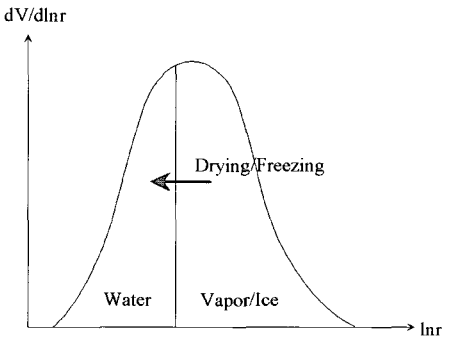

Fig. 4 Freezing or drying in pore distribution (volume/logarithmic radius of pores)

$$\Delta(\Delta\mu) = \int_{Tref}^{T} (S_{m,s}(T) - S_{m,l}(T))dT =$$

$$0.0997T^2 - 76.4532T + 13444483 \quad (25)$$

where, the surface tension varies temperature dependently as follows.

r_s(L1): Surface tension by extrapolating the value of -1 to -40°C, calculates Thus, the value of the surface energy at different temperatures may be estimated from [5]:

$$\gamma_{S-L} = \frac{33 + 0.2T}{1000} \text{ mJ/m}^2 \quad (26)$$

r_s(L2): considering spontaneous freezing of small water droplets[6],

$$\gamma_{S-L} = 0.0305\{1 - 0.0093(T_o - T)\} \text{ mJ/m}^2 \quad (27)$$

The difference in chemical potential between the liquid and the solid phase

r_s(L3): Substituting γ_{S-L} of Eq.26 to Eq.24.

r_s(L4): Substituting γ_{S-L} of Eq.27 to Eq.24.

Consequently, integrating Eq.22, the amount of freezable water can be calculated for various water to cement ratios (w/c), shown in Fig. 5, (Unit: cc/g).

Shown in the Fig. 5, from the calculation of freezable water at each temperature drops, the freezable radius of pore is inversely proportional to temperature.

The freezable water will increase from 0 value as the temperature drops. In addition, the final value might be close to the whole amount of water in concrete. Thus, in the developed numerical code, equation of L3 case has been selected for the evaluation of the amount of ice in concrete.

3.3 Ice expansion in micro pores

The interfaces between water-vapor and water-ice show similar growth, even though the driving sources are different as humidity and temperature. When drying, the difference between increased vapor pressure and decreased liquid pressure makes the volume of vapor bigger (Fig. 6(A)). Similarly, when temperature drops, the difference between increased solid (freezing) pressure and decreased liquid pressure makes the volume of ice bigger (Fig. 6(B)). By those increased pressures, the vapor/solid will penetrates to smaller pore, which has smaller radius until new equilibrium meets. In the figures, the movements in the distribution of pores, with changed distribution of water or solids are shown in the distribution diagram also.

Considering the equilibrium of chemical potential, the growth of ice to pore can be obtained:

$$\Delta\Omega = -SdT - pdV + \gamma dA = 0 \quad (28)$$

In isothermal condition, $dT = 0$, thus,

$$p_{LS}dV = \gamma_{SL}dA \quad (29)$$

With the increase of p_{LS}, dA is needed to be increased for equilibrium, thus the interface angle will be decreased with the increase of interface area, where γ_{LV}: Liquid-Vapor surface tension, γ_{SL}: Solid-Liquid surface tension, and θ contact angle between interfaces.

3.4 Driving force of freeze

The molar Gibbs free energy (chemical potential) of ice and water are like the following:

For bulk water:

$$\mu_l(T,P) = \mu_l(T,P) + V_l\Delta P_f = \mu_l(T) + \int_{T_O}^{t}\{-S_l(T)\}dT + V_l\Delta P_f \quad (30)$$

For brine water[7]:

$$\mu_l(T,P) = \mu_l(T,P) + V_l\Delta P_f + RT\ln(X_l) = \mu_l(T) + \int_{T_O}^{T}\{-S_l(T)\}dT + V_l\Delta P_f + RT\ln(X_l) \quad (31)$$

The main assumptions used for the derivation of driving forces are as follows:

1) In highly saturated pores, ice expansion pressure brings higher stresses in frozen concrete. Thus, material follows nonlinear-fracture constitutive law.

Table 1 The minimum freezable radius with various surface tension formulas (Unit: m)

T(°C)	r_s(L1)	r_s(L2)	r_s(L3)	r_s(L4)	r_s(Mihashi)
-5	2.99E-08	1.00E-08	3.03E-08	1.02E-08	1.76E-08
-10	1.56E-08	5.05E-09	1.46E-08	4.73E-09	9.31E-09
-20	8.58E-09	2.55E-09	6.85E-09	2.03E-09	5.24E-09
-30	6.35E-09	1.71E-09	4.28E-09	1.15E-09	3.97E-09
-40	5.37E-09	1.29E-09	3.01E-09	7.24E-10	3.44E-09
-50	4.92E-09	1.04E-09	2.26E-09	4.76E-10	3.24E-09
-60	4.82E-09	8.59E-10	1.77E-09	3.16E-10	3.25E-09

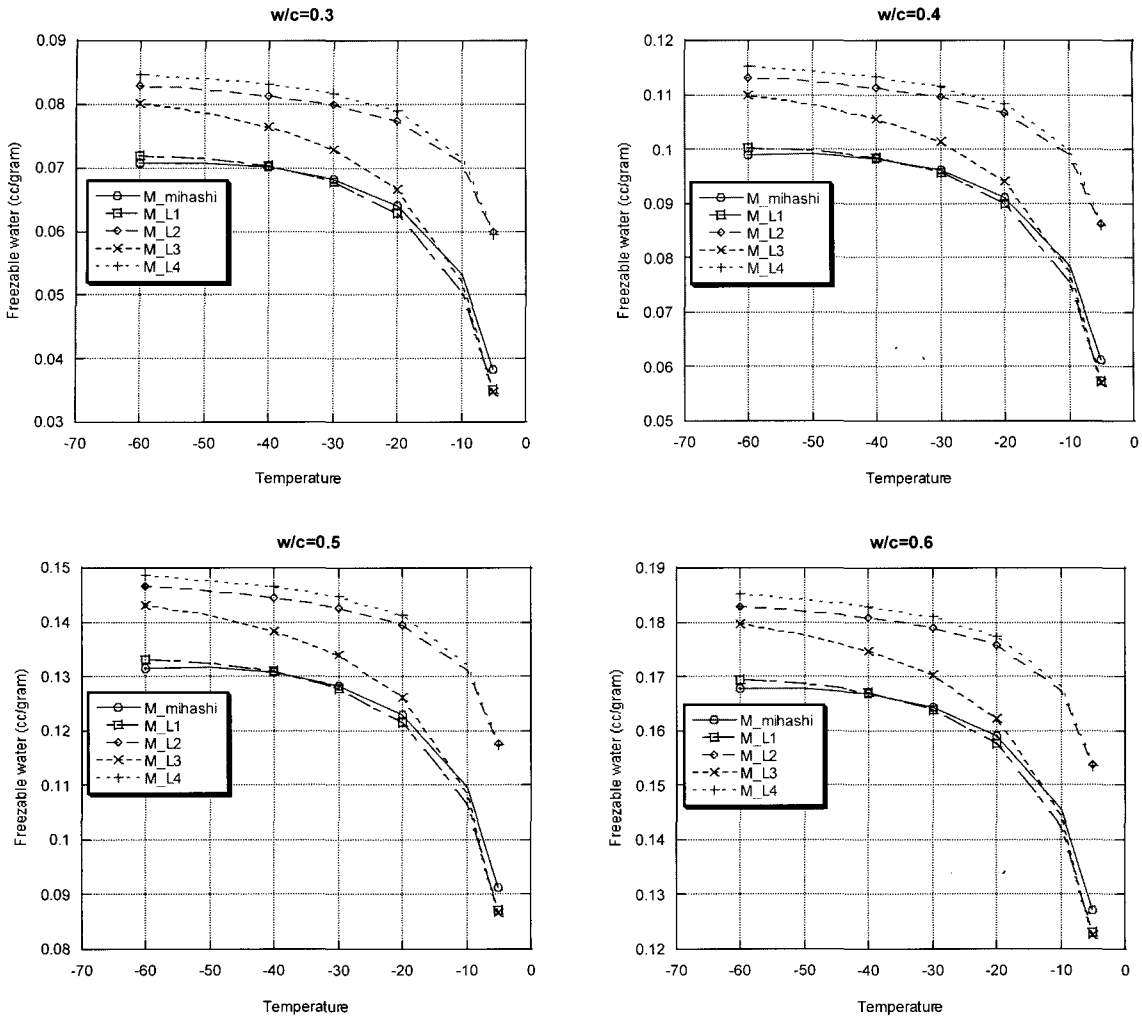

Fig. 5 The freezable water with the variation of w/c ratio

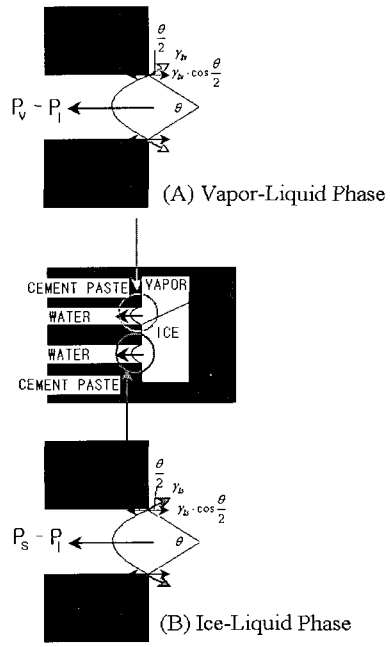

Fig. 6 Two phase equilibrium

2) Fully saturated gel pore begets much bigger ice expansion pressure than partially saturated case.
3) By the ice expansion pressure, pore volumes are increased. Thus, the saturation of ice and pressure are decreased.
4) Strain by thawing is obtained by the different thermal expansions of water, ice, cement paste, and aggregates.

For the potential of ice:

$$\mu_s(T,P) = \mu_s(T,P) + V_s\Delta P_f = \mu_s(T) + \int_{T_O}^{T}\{-S_s(T)\}dT + V_s\Delta P_f \tag{32}$$

By equating the two potential statuses, the pressure in bulk water can be obtained

$$\Delta P_f = \frac{-\int_{T_O}^{t}\{S_l(T)-S_s(T)\}dT}{V_s} + \frac{RT\ln(h)}{V_s} = \frac{-\int_{T_O}^{T}\frac{\Delta_{fus}H}{T}dT}{V_s} + \frac{RT\ln(h)}{V_s} \tag{33}$$

And the pressure in brine water can be obtained:

$$\Delta P_f = \frac{-\int_{T_o}^{t}\{S_l(T)-S_s(T)\}dT + RT\ln(X_l)}{V_s} = \frac{-\int_{T_o}^{T}\frac{\Delta_{fus}H}{T}dT}{V_s} + \frac{RT\ln(h)}{V_s} + \frac{RT\ln(X_l)}{V_s} \quad (34)$$

where the heat of fusion is approximately assumed as follows:

$$\Delta_{fus}H = \frac{6010}{T_o} - 40\ln\left(\frac{T_o}{T_{curr}}\right) \text{ (J/mol)} \quad (35)$$

4. Numerical model

4.1 Nonlinear-fracture constitutive relationship

In the Fig. 7, normalized stress-strain are obtained from Eq.36. Under cyclic loads, a specimen shows decreased strength and stiffness. The decreased stiffness can be expressed as a damage index K, as the statistical fracture index[8].

$$S = E_o \cdot K \cdot E_e : \text{Normalized Stress} \quad (36)$$

where E_o(=2.0): Initial Stiffness, K(=exp(-0.73·E_{max}(1-exp(-1.25·Emax)))): Statistical Fracture Index, E_e(=E-E_p): Equivalent Strain, E_p (=E_{max}-(20/7)(1-exp(-0.35·E_{max}))):Plastic Strain, and E_{max}: the updated maximum strain in those hysteric cycles considered.

In the given equations, the fracture index (K) is considered to be a function of equivalent maximum strain. It had been obtained by fitting the experimental data. As the damage in concrete by any cyclic load increases, the mechanical equivalent plastic strain also increases. This phenomenon happens because the higher the damage is, the lesser compression the elements carry. These elements reach their plastic point more quickly resulting in a higher mechanical plastic[9].

4.2 Micro cracking model

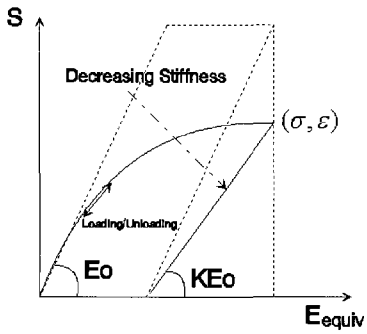

Fig. 7 Normalized stress-strain relationship considering nonlinear-fracture[8]

To predict the length of micro-cracking by frost actions as an evaluation of micro cracking, based on fracture mechanics, the stress intensity factor has been considered[4]:

$$K_{IC} = \frac{\Pr^2}{\sqrt{\pi}C^{2/3}} \quad (37)$$

where, K_{IC} is the mode I stress intensity factor of the porous material. When pore has an enough internal freezing induced pressure P, the pore will show crack length of 2C in Mode I.

$$\delta = \pm\frac{K_{IC}}{2G}\sqrt{\frac{C}{2\pi}}(1-\nu) \quad (38)$$

The increased crack length is obtained by double the crack half length C (Eq.38), with the G (the modulus of rigidity), C, and K_{IC}, considering symmetric condition; we can obtain the total displacements.

Considering the distribution of micro pores, it can be calculated the whole the increased pore volume in various way. One of the methods can be direct integration using the distribution density function as the following:

$$\delta_{total}(T) = \frac{\sqrt{2}(1-\nu^2)K_{IC}^{2/3}}{E\pi^{2/3}}(-302.3\ln(\frac{T}{T_O}))^{1/3}\int_i^{\max} r^{2/3}q_i(r)dr \quad (39)$$

In the considered equation above, as expressed as unequal signature, there might be a problem of dimension, while integrating. Therefore, the authors propose another numerical method: The individual crack propagation and volume increase in micro-pores are obtained by the integration of Eq.39, by the use of distribution function shown in the Fig.8.

$$d_{total}(T) = \sum\frac{\sqrt{2}(1-\nu^2)K_{IC}^{2/3}}{E\pi^{2/3}}(S\cdot\Delta P_f\cdot V_i(T))^{1/3}r_i^{2/3} \quad (40)$$

Where, Vi(T): volume of ice at temperature T(Eq.56)

Increased Pore Volume (Volume_cone)=$(2\pi\frac{r_i}{3})(\frac{d(I)}{2}+r_i)^2$

Initial Pore Volume (Volume_sphere)=$(4\cdot3.11592\frac{r_i^3}{3})$

N=$\frac{\phi\{\exp(-Br_b)-\exp(-Br_c)\}}{\text{Volume\_sphere}_i}$: Number of air pores in a divided section (Fig. 8).

Using fracture mechanics, the macroscopic deformation can be evaluated like the following:

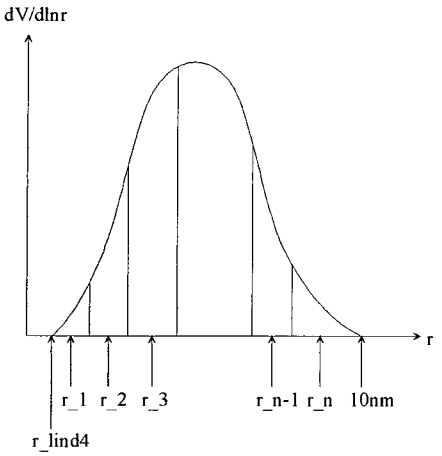

Fig. 8 Proposed density function of micro pores

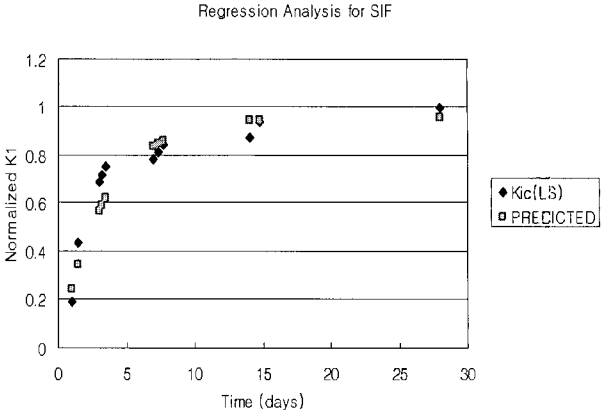

Fig. 9 Obtained stress intensity factor from experimental results

r_i: the minimum freezable radius was used

r_{max}: 0.0001 meter is assumed

K_{IC}: obtained from the regression analysis (Fig. 9)

Finally the total increased pore volume is:

Δ Volume =(Volume_cone- Volume_sphere)

Finally, the increased Volume=$\sum_{\Delta}$ Volume

Where, the Stress Intensity Factor is calculated from the regression analysis of the experiments done by Kim and et al. [10].

For OPC,

K_{IC}=0.955284*{exp(4.2e-5T)-exp(-0.298908T)}*(5.144-4.995*w/c) (41)

For silica fumed,

K_{IC}=0.955284*{exp(4.2e-5T)-exp(-0.298908T)}*(4.839-4.844*w/c) (42)

Where, T is time (days), and 0< w/c: (%/100) <1.

4.3 Increased pore volume

Due to the different ice expansion pressure, which depends saturation, the pores need to be considered respectively. Dividing capillary and gel pores, the increase of pore volumes and saturation have been evaluated separately and updated as follows:

1) Pore volume of capillary pores:

$$V_{CP} = \exp\left(-B_{CP} \cdot r_{L3}\right) \tag{43}$$

2) Equivalent radius of capillary pores:

$$r_{eq\_CP} = -\left(\frac{1}{B_{CP}}\right) \ln\left(V_{CP}\right) \tag{44}$$

3) Increased pore volume of capillary pores (Refer to Eq. 40):

$$\Delta V_{CP} \tag{45}$$

4) The normalized increased pore volume of capillary pores:

$$\phi_{CP} = \phi_{CP}\left(1 + \Delta V_{CP}\right) \tag{46}$$

5) The updated B factor:

$$B'_{CP} = -\left(\frac{1}{r_{eq\_CP}}\right) \ln\left(V_{CP} + \Delta V_{CP}\right) \tag{47}$$

6) Pore volume of capillary pores:

$$V_{GL} = \exp\left(-B_{GL} \cdot r_{L3}\right) \tag{48}$$

7) Equivalent radius of capillary pores:

$$r_{eq\_GL} = -\left(\frac{1}{B_{GL}}\right) \ln\left(V_{GL}\right) \tag{49}$$

8) Increased pore volume of capillary pores (Refer to Eq. 40):

$$\Delta V_{GL} \tag{50}$$

9) The normalized increased pore volume of capillary pores

$$\phi_{GL} = \phi_{GL} \cdot \left(1 + \Delta V_{GL}\right) \tag{51}$$

10) The updated B factor:

$$B'_{GL} = -\left(\frac{1}{r_{eq\_GL}}\right) \ln\left(V_{GL} + \Delta V_{GL}\right) \tag{52}$$

where the increased pore volumes should have to be updated after each free-thaw cycles (Fig. 8).

4.4 Effect of entrained air pores: Power's spacing factor and hydraulic pressure

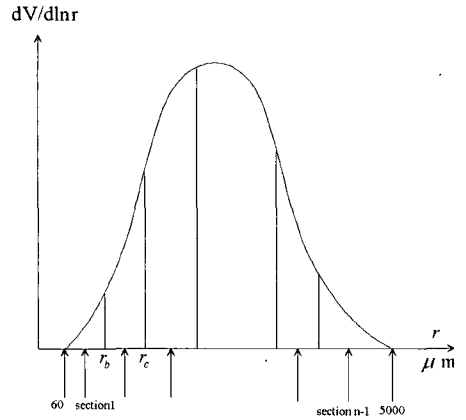

Fig. 10 Proposed density function of entrained air pores for numerical model

Excessive water caused by freezing has to flow from saturated areas to air-filled spaces. This flow creates a hydraulic pressure, which in turn, produces tensile stresses in the material. The hydraulic pressure p (Pa) inside the material sector considered is[11];

$$P=\frac{0.09}{K}\frac{dw_f}{dT}\frac{dT}{dt}\int_0^X\frac{v(x)}{a(x)}dx \tag{53}$$

Where, K: the effective permeability (m^2/(Pa•s)), dw_f/dT the change in freezable water at a change in temperature (m^3/m^3 degree)), dT/dt the rate of temperature lowering (the freezing rate) (degree/s), v(x) the volume of the sector considered between x=x and x=X, $v(x)=(4/3)\ \pi\ \{(r+L)^3-(r+x)^3\}$, X is the distance from the surface of the piece to point C, a(x) cross section of flow at x=x, $=4\pi(r+x)^2$.When p=f_t, tensile strength of the concrete, the material fractured. Thus, for a slice thickness D, the critical thickness D_{cr} is (a(x) =a; v(x) =a(D_{cr}/2-x));

$$D_{cr}=4\pi(r+x),\ v(x)=(4/3)\ \pi\ \{(r+L^3)^2\}\ (m) \tag{54}$$

L is length to the nearest air pore (Power's spacing factor), L_{cr} is (Power's) critical flow distance, length where the unfrozen water can move, when S = S_{cr}, a is the air content of the cement paste(m^3/m^3), α is the specific area of the air-pores (m^2/m^3), f_t is the tensile strength of the cement paste, K is the permeability, $\frac{dw_f}{d\theta}$ is the freezing rate (Mass/Temperature), and $\frac{d\theta}{dt}$ is freezing rate (Temperature/Time).

For a distribution model of entrained air pores, the following assumptions have been considered:

1) Unfrozen smaller air pores are filled first (considering spacing factor)
2) The pore volumes are increased by the ice expansion pressures (Eq. 37).
3) The porosity of ITZ is approximately 1.5 times of the porosity of capillary pores[12].

4.5 Structural deformation

The total freezing deformation can be given by the sum of each deformation and the sum of thermal expansion with the resisting effects of entrained air pores:

$$\varepsilon_{tot}=\varepsilon_\sigma-\varepsilon_K-\varepsilon_t-\varepsilon_{AE}=\frac{\Delta P_f V_i(T)}{E_s}-\frac{\Delta P_{LS}V_w(T)}{K_s}-\alpha\Delta T-\varepsilon_{AE} \tag{55}$$

where the considered strains are ε_{tot}: total strain, ε_σ: expansion strain[4], ε_K: contraction strain by micro-ice-lens theory[13], ε_t: thermal contraction strain considering 4 materials, which are ice, water, cement and aggregates, and the volume of unfrozen water, $V_w(T)$, will be the difference of V_{tot}-V_i. The volume of ice is:

$$V_i(T)=\phi_{cp}\int_{ri}^{r\max}B_{cp}\exp(-B_{cp}r)dr+\phi_{gl}\int_{ri}^{r\max}B_{gl}\exp(-B_{gl}r)dr \tag{56}$$

The fractional pore volume of the distribution (cc/g) is:

$$V_{tot}=\phi_{cp}\int_{r\min}^{\infty}\exp(-B_{cp}r)dr+\phi_{gl}\int_{r\min}^{\infty}\exp(-B_{gl}r)dr \tag{57}$$

$$=\phi_{cp}\exp(-B_{cp}r_{\min})+\phi_{gl}\exp(-B_{gl}r_{\min}) \tag{58}$$

where, ΔP_f is obtained from Eq.33 and Eq.34, and $\Delta P_{LS}=1.22(1+3\cdot10^{-3}\theta)\cdot\theta$ [13], θ: temperature in Celsius, respectively.

The reduced strain by the effect of entrapped and entrained air pores, ε_{AE}, the volume of ice (m^3/m^3) depends on the distribution of gel pore and capillary pores in each section from the distribution: The distribution of entrapped and entrained air pores were modeled as:

If the air pores are 2%,

$$V_o=\int_{60\mu m}^{\infty}B_{AE}r\exp(-B_{AE}r)d\ln r=1-\exp(-B_{AE}r)=0.02\ (=2\%) \tag{59}$$

where the diameter of entrapped air pores: 2000-5000 μm, the diameter of entrained air pores: 60-1000 μm, distribution factor of entraiend air:B_{AE}(2%)=2000, and B_{AE}(7%)=7257.07 when the average of the radius of entraiend air pores is r_{avg}=138 μm.

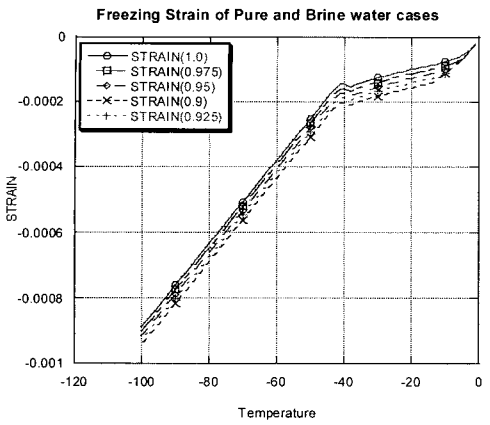

Fig. 11 Freezing strain of pure and brine water

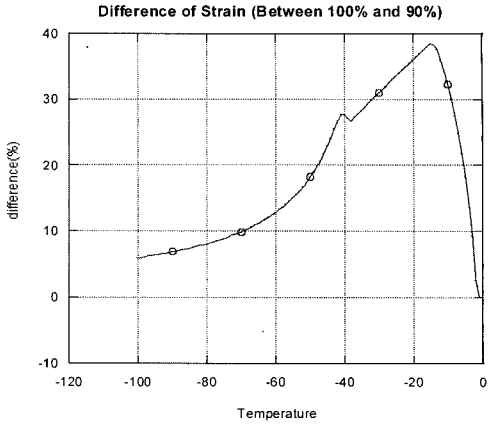

Fig. 12 Difference of strain (0 and 10% of Solutes)

5. Simulation results

A subroutine for the analysis of freezing and thawing has been developed, including all the previous discussions. The developed program can be combined with the DuCOM (Section 3.1). Therefore, the developed model can be applied to evaluate those various practical degradation cases also. As verification, various numerical simulations have been conducted for the parameters of the content of chloride, water to cement ratio, amount of entrained air pores, and amounts of aggregates. The mix proportions and model parameters are shown in Table 2. The analysis results are presented and discussed in this section.

5.1 The effect of the content of chloride

As discussed for the chemical potential of pure and brine water (Eq.31 and Eq.34), as the increased solutes, the chemical potential decreases. As a result, (Fig. 11) while solutes increase from 0 to 10%, the differences of nonlinear strain of the surface of specimen in the numerical simulations show 0 to 39% differences as a maximum difference. In addition, the difference is decreased as the increased ice formation in gel pores (Fig. 12). However, this reduction does not mean beneficial effect. Because the "not-yet-frozen water" will flow to the nearest ice in bigger pores, which result bigger ice expansion and cracking at the pores. In addition, free water will transfer chloride ions to the reinforcements and accelerating corrosions.

Table 2 Mix proportions and pore distributions of three simulation cases

Mix	M60	M50	M35	Comments
w/c	4.00E-01	6.00E-01	6.00E-01	kg/kg
Entrained air Pores	6.50E-02	8.00E-03	8.40E-02	%
B_{cp}	8.90E+06	3.91E+06	3.91E+06	B parameter
B_{gl}	6.04E+07	6.06E+07	6.06E+07	B parameter
B_{AE}	6.72E+03	8.03E+02	8.77E+03	B parameter
$R_{AE)avg}$	1.49E-04	1.25E-03	1.14E-04	Meter
ϕ_{cp}	7.10E-02	1.46E-01	1.21E-01	Capillary porosity
ϕ_{gl}	6.40E-02	6.90E-02	5.70E-02	Gel porosity
ϕ_{tot}	2.00E-01	2.23E-01	2.62E-01	Total porosity

5.2 The effect of water to cement ratio

The higher water to cement ratio specimen (M35) have 30 % higher porosity than the lower one (M60). This also gives higher freezable water. As a result, shown in the Figs.13 and 14, the difference of nonlinear strain of the surface of specimen in the higher w/c case shows 97% larger strain as a maximum difference than the lower w/c case. It also shows reducing difference while gel pores are freezing, as temperature is decreased lower than -40°C.

5.3 The effect of entrained air pores

The amount of aggregates decreases with the increased entrained air pores. Comparing 0.8% (M50) and 8.4% (M35) EA cases, the Figs. 15 and 16 shows the difference of nonlinear strain of the surface of specimen 70% differences as a maximum difference.

Although, this absorption ability or buffer effect to the freezing shrinkage is reducing under large number of cyclic freeze-thaw, when there is enough water supplying from the outside of concrete[9], it is the second largest factor, which is effective to the resistance of concrete to freeze-thaw, observed in this research.

5.4 The increased pore volumes

The sensitivity of water to cement ratio can be shown by

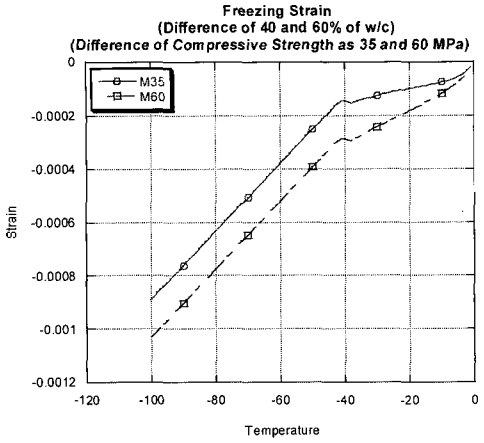

Fig. 13 Freezing strain in different w/c

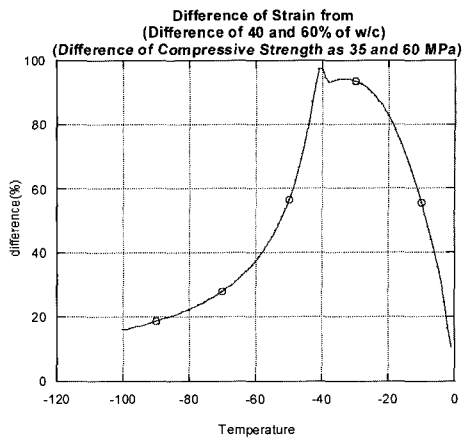

Fig. 14 Difference of strain

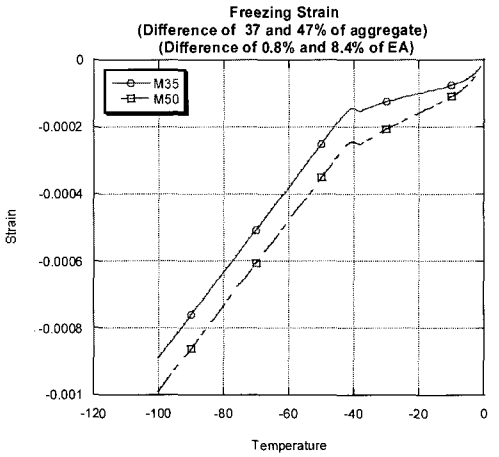

Fig.15 Freezing strain with entrained air pores

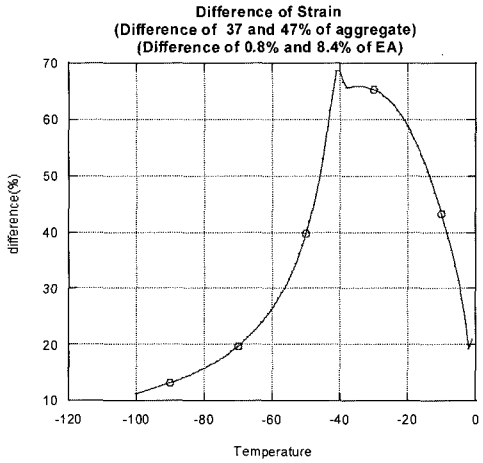

Fig.16 Difference of strain

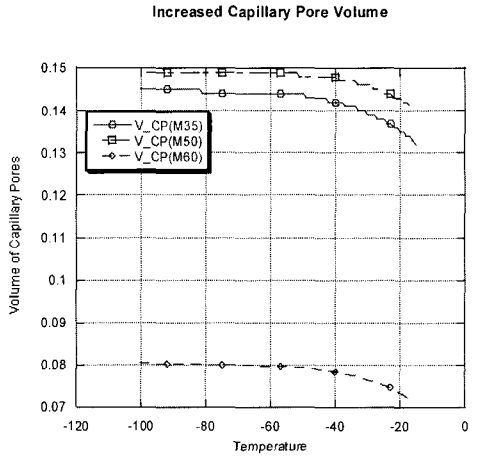

Fig. 17 Increased capillary pore volume

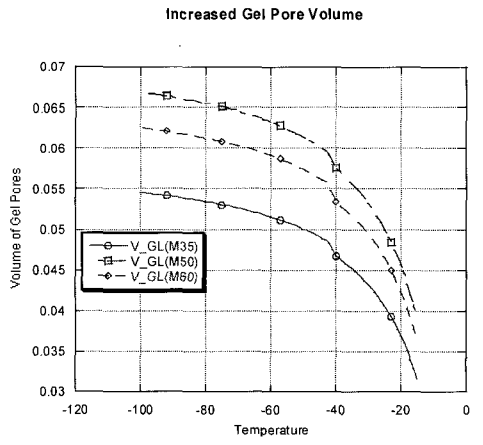

Fig. 18 Increased gel pore volume

plotting the increased capillary pores by the ice expansion pressure. Even though entraining enough air pores (EA=8.4%, M35), due to the larger amount of freezable water, it shows higher increased capillary pore volume (Fig. 17). Meanwhile, the gel pore volume shows less sensitive to water to cement ratio, but shows higher sensitivity to entrained air pores. It might come from the distribution of micro pores. In the distribution factors (Table 2), between M50 and M60, the difference ratio of the average radius of capillary pores is 56%, and the difference ratio of B parameter of capillary pores is 127% respectively. While the difference ratio of the average radius of gel pores is 0.36%,

and the difference ratio of B parameter of gel pores is 0.33 % respectively. Therefore, the amount and distribution of gel pore is not sensitive to the water cement ratio.

However, the unfrozen water will flow from smaller pores to the entrained air pores while larger pores are freezing. As can be seen in the Fig. 18, the difference of 7.6% of entrained air pores shows over 20% increased gel pores, which is the result of the propagation of micro cracks (Section 5.2).

6. Conclusions

The following summarizes the discussed freeze-thaw induced deterioration problems of concrete structures:

1) A numerical code has been developed for the evaluation of cyclic freeze-thaw effects in concrete structures, which has the features of (a) Expansion behavior due to the internal pressure caused by phase transition (b) Three types of ice expansion pressure are modeled which depends on the saturation of micro-pores, based on thermodynamics. (c) Deformation, freezing shrinkage, due to thermal contraction and water transportation has been modeled numerically.
2) To predict the amount of freezable water, temperature dependent surface tension and heat of fusion have been considered for the evaluation of freezable water. Numerical simulation for a the freeing has been carried from 0 to -100 ^{O}C for various cases of water to cement ratio, entrained air pores and solutes.
3) For obtaining the reduced saturation, fracture mechanics based increased pore volume have been calculated in cement paste and mortar, which are updated at each drop of temperature. With the proposed distribution of air pores, instead of previous model by integration, the authors propose numerical method: The individual crack propagation and volume increase in micro-pores are obtained by the summing up for all the micro pores (Eq.40, Fig.8).
4) As a simulation result, the effect of the content of chloride shows 39% reduced freezing shrinkage strain, when 10% of chloride ions added to the pure water. However, this reduction does not mean beneficial effect. Because the "not-yet-frozen water" will flow to the nearest ice in bigger pores, which result bigger ice expansion and cracking at the pores.
5) The effect of the water to cement ratio shows significant sensitivity to the distribution of capillary pores (bigger pores). The higher water to cement ratio specimen has higher porosity than the lower one. This also gives higher freezable water. As a result, the difference of nonlinear strain of the surface of specimen in the higher w/c case shows 100% larger strain as a maximum difference than the lower w/c case.
6) Meanwhile, the w/c is not so sensitive to the gel pores (smaller pores), because the increased gel pore volume, due to the ice expansion pressure, shows less sensitive to water to cement ratio, but shows higher sensitivity to entrained air pores. Compared with capillary pores, the distribution of gel pores is less sensitive to the w/c. However, the unfrozen water will flow from smaller pores to the entrained air pores while larger pores are freezing. The difference of 7.6% of entrained air pores shows over 20% increased micro pores, which is the result of the propagation of micro cracks.

References

1. Setzer M., *Modeling and testing the freeze-thaw attack by micro-ice-lens model and CDF/CIF test*, Micro-structure and durability to predict service life of concrete structures, 2004, pp.17~27.
2. Maekawa K., Kishi T., "Multi-Component Model for Hydration Heating of Portland Cement", *JSCE,* Vol.29, No.526, 1995, pp.98~112.
3. Zhu Y.B., *Multi-scale constitutive model of concrete based on thermodynamic states of moisture in micro*, Thesis of the University of Tokyo, 2004, pp.36~41.
4. Mihashi H., Z. Y. Zhou, *Micro mechanics model to predict macroscopic behavior of concrete under frost action*, RILEM proceedings PRO24, 1997, pp.235~241.
5. Hobbs, J.P., C.S.P. Sung, K. Krishnann, and S. Hill, "Characterization of surface structure and orientation in polypropyl-ene and poly(ethylene terephthalate) films by modified attenu-ated total reflection IR dichromism studies," *Macromolecules*, 16, 1983, pp.193~199.
6. Hesstvedt, E., *The Interfacial Energy Ice/Water*, Norges Geotekniska Institutt, Publikasjon nr. 56, Oslo, 1964, pp.823~833.
7. Wolfe J.and Bryant G., "Cellular cryobiology: thermodynamic and mechanical effects", *International Journal of Refrigeration*, Vol.24, Issue5, 2001, pp.438~450.
8. Maekawa K., Pimammas A., and Okamura H., *Nonlinear Me-chanics of Reinforced Concrete*, Spoon Press, 2002, pp.431~564.
9. Ueda T., M. Hasan, K. Nagai, and Y. Sato, *Prediction of structural performance during service life from microstructure*, Microstructure and durability to predict service life of concrete structures, 2004, pp.39~50.
10. Kim J. Lee Y., Yi S., "Fracture characteristics of concrete at early ages", *Cement and Concrete Research,* Vol.34, 2004, pp.39~50, 507~519.
11. Powers, T.C, *Freezing Effects in Concrete, in Durability of Concrete*, ACI SP-47, 1975, pp.1~11.
12. Bentz, D.P., Garboczi, E.J., and Stutzman, P.E., "Computer Modelling of the Interfacial Zone in Concrete", I*n Interfaces in Cementitious Composites*, Ed. J.C. Maso, 18, 1992, pp. 39~50, 107~116.
13. Setzer M., "Micro-Ice-Lens Formation in Porous Solid", *Journal of Colloid and Interface Science,* 243, 2001, pp.39~50, 193~201.